Proceedings of the ASME 2022 41st International Conference on Ocean, Offshore and Arctic Engineering
OMAE2022
June 5-10, 2022, Hamburg, Germany

OMAE2022-79016

A COUPLED WAVE-CURRENT-STRUCTURE STUDY FOR A FLOATING OFFSHORE WIND TURBINE PLATFORM

Xiang Li
Department of Naval Architecture, Ocean and Marine Engineering, University of Strathclyde, Glasgow, UK

Qing Xiao
Department of Naval Architecture, Ocean and Marine Engineering, University of Strathclyde Glasgow, UK

Rodolfo T. Gonçalves
OSPL - Ocean Space Planning Laboratory, Department of Systems Innovation, School of Engineering, The University of Tokyo, Tokyo, Japan

Christophe Peyrard
Saint-Venant Hydraulics Laboratory (Électricité de France, ENPC), Université Paris Chatou, France

ABSTRACT

In the present study, the influence of ocean conditions, in the combination of wave and current, on the dynamic response of the OC4 semi-submersible platform is numerically studied. The present work is inspired by the recent observations that the presence of current incidence usually induces the vortex-induced motions (VIM) phenomenon of multi-monocolumn platforms, while wave often leads to large inertia force on it. The integration of wave and current may further cause a more complex flow field around the structure than that only wave or current exists. Such VIM is not desirable considering its impact on the fatigue life of the riser, umbilical, and mooring system of the offshore structure due to the resonance behaviour of the VIM.

A computational fluid dynamic (CFD) method is adopted to conduct a real-time simulation of the platform's motion response. The tool is based on an open-source code library OpenFOAM. The results are validated against experiments with current-only conducted in the wave tank. The flow field around the platform and its impact on the structure motion and loading response are studied for a wide range of wave and current conditions. With the given incident waves, the VIM is mitigated for most cases, for a wide range of reduced velocity. This result is of practical interest for the design of FOWT, as VIM are not captured by industrial aero-hydro-mechanical models.

Keywords: Vortex-induce motions (VIM), Floating Offshore Wind Turbine (FOWT), OC4 platform, OpenFOAM

1. INTRODUCTION

Floating offshore wind turbine (FOWT) is getting more attention due to the practical need to deploy wind energy devices in deeper water. With the application of larger and taller turbine towers, the supporting platform is more vulnerable to extreme sea conditions. For example, wave loads induce large inertia forces on the floating structures, meanwhile current usually leads to vortex-induced motion (VIM). Therefore, the influence of coupled wave-current is important for the dynamic response of the FOWT.

VIM of cylinders and monocolumn platforms has been widely studied [1-5], which is found to be deeply related to its structural natural frequency and vortex shedding frequency. The vortex-induced vibration (VIV) response is also studied, and the classic 8-shaped orbital trajectories are found for typical cases. This low-frequency response, especially in cross-flow direction, may result in potential damage to FOWT's mooring systems and cause fatigue problems [6]. The VIM phenomenon is much more complicated for semi-submersible platforms, due to their large dimension and multi-column structure with wakes interacting with each other. The phenomenon also differs with different geometry of platforms. Gonçalves studied experimentally the VIM of OC4 FOWT platform and semi-submersible platform

with four square columns [7, 8]. The cross-flow motion response varies with different incident angles of current for both platforms. Given the different geometry of platforms, the reduced velocity V_r at which VIM occurs both falls between 4.0 and 14.0, with different ranges of peak responses. The influence of draft and damping is also studied which is proved to have an obvious effect on VIM.

Computational Fluid Dynamic (CFD) is one of the useful tools for VIM study because it can easily obtain the flow field information, e.g., velocity and pressure field and vortex structure. Kim et al. [9] conducted preliminary simulations to predict the VIM of a TLP design using STAR CCM+ and compared with the physical model test results. Zhao et al. [10] studied VIM of semi-submersible platforms using the CFD method. The vortex shedding frequency is found to increase with current velocity and not locked on one natural transverse frequency. Huang and Chen [11] investigated the mooring-induced damping effects on VIM using coupled CFD-FEM method, their findings show that the mooring-induced damping effects represent a dominant contribution to the reduction in VIM transverse motion in both lock-in and post-lock-in regimes.

Given a real operation condition, ocean current is usually accompanied by ocean waves, and this may bring new variables for the VIM phenomenon. However, very rare studies on VIM with the presence of waves can be found. Maximiano et al. [12] studied irregular waves and current interaction with SS platforms experimentally. Their results reveals the wave-induced particle velocity disturbs the VIM, which is strongly dependent on the incident wave height. The VIM is mitigated by the occurrence of waves at larger wave height, up to 30% with the highest wave height in their experiment. Gonçalves et al. [13, 14] performed a more in-depth VIM test of the SS platform with a variety of wave and current conditions. With both regular and irregular wave conditions, they found VIM phenomena, and the motion response is linked to Keulegan-Carpenter number *KC* and velocity ratio α', here, the *KC* number is a parameter to determine if the flow is viscous or inertia dominant

To the author's knowledge, there is no CFD research on this topic is published. In this study, the influence of an ocean condition, in a combination of wave and current, on the dynamic responses of the OC4 FOWT platform is numerically studied. A high-fidelity CFD method is utilized to solve this fluid-structure-interaction (FSI) problem, which makes it possible for a deep understanding of the flow field associated with VIM.

2. MATERIALS AND METHODS

2.1 Flow Model

The simulation of the VIM of the OC4 platform fluid-structure interaction problem is performed based on the OpenFOAM code. The multi-phase flow solver OlaFlow is used which is developed on top of OpenFOAM, providing powerful wave generating boundary and active wave absorbing boundary. In this model, the incompressible Naiver-Stokes equations are solved:

$$\nabla \cdot U = 0 \tag{1}$$

$$\frac{\partial \rho U}{\partial t} + \nabla \cdot \left(\rho \left(U - U_g \right) U \right) = -\nabla P_d - g \cdot x \nabla \rho + \nabla \left(\mu_{eff} \nabla U \right) + \left(\nabla U \right) \cdot \mu_{eff} + f_\sigma \tag{2}$$

where U and U_g is the velocity of the fluid and CFD grid, respectively, and ρ is the fluid density. P_d denotes the dynamic pressure. x is the coordinate, g is the gravity acceleration. μ_{eff} denotes the effective dynamic viscosity, f_σ is the surface tension which is only considered on the free surface.

The Volume of Fluid (VoF) method is applied to solve the two-phase flow problem. The volume fraction α is governed by the following transport equation:

$$\frac{\partial \alpha}{\partial t} + \nabla \cdot \left(\left(U - U_g \right) \alpha \right) + \nabla \cdot \left(U_r \left(1 - \alpha \right) \alpha \right) = 0 \tag{3}$$

For a multi-phase flow problem, fluid density and viscosity can be written as a mixture of water and air:

$$\rho = \alpha \rho_w + \left(1 - \alpha \right) \rho_\alpha \tag{4}$$

$$\mu = \alpha \mu_w + \left(1 - \alpha \right) \mu_\alpha \tag{5}$$

where ρ_w and ρ_a denote the density of water and air, μ_w and μ_a denote the viscosity coefficient of water and air.

To generate numerical waves, the fluid velocity at the inlet boundary is prescribed using Stokes second-order wave theory:

$$u = \frac{\pi H}{T} \frac{\cosh k\left(z + d \right)}{\sinh kd} \cos\theta + \frac{3\pi H}{4T} \left(\frac{\pi H}{L} \right) \frac{\cosh 2k\left(z + d \right)}{\sinh^4 kd} \cos 2\theta \tag{6}$$

$$w = \frac{\pi H}{T} \frac{\sinh k\left(z + d \right)}{\sinh kd} \sin\theta + \frac{3\pi H}{4T} \left(\frac{\pi H}{L} \right) \frac{\sinh 2k\left(z + d \right)}{\sinh^4 kd} \sin 2\theta \tag{7}$$

where H and T denote the wave height and wave period, k and d denote wave number and water depth, θ is the phase. For a complete description of the theory of wave generation and absorbing, the readers are referred to olaFlow manual. For wave-current study, the particulars' velocity at this boundary is given by the superstition of current speed and particulars' speed given by the wave theory. In this paper, no superstructures and wind load are considered, and no turbulence model is used.

2.2 Structural Model

The dynamic response of the OC4 platform is governed by the following motion equations:

$$m\ddot{x} + c\dot{x} + kx = F_x \tag{8}$$

where x denotes the translational motion of the platform, m, c and k represent the platform mass, structural damping coefficient, and spring stiffness, respectively. F_x denotes the hydrodynamic force acting on the platform. The Newmark-beta method is adopted to solve Eq. (8) for the motion of the cylinder. To make the simulation stable, an acceleration relaxation factor of 0.7 is adopted. Since we focus on the transverse VIM motion of the platform, only x and y degrees of freedom are considered.

2.3 Experimental model

The scaled-down OC4 semi-submersible platform model in this paper is based on the 1:72.72 model test performed at the University of Tokyo by Gonçalves et al [8]. The test aimed to study the VIM of the OC4 platform with current interaction. The dimensions of the towing tank were 85m in length, 3.5m in width, and 2.4m in depth. The platform is made up of four columns, one main column with a smaller diameter in the centre and three offset columns with larger diameters. Columns are connected with crossbars in between. There are base columns attached below the side columns. The details of the geometric parameters can be found in Table 1. The model is restrained by four perpendicular mooring lines and the equivalent stiffness of the mooring system are also shown in Table 1. The natural frequency is obtained via the free decay test, the natural frequency along in-line and cross-flow direction is 9.4s and 9.6s, respectively.

FIGURE 1: OC4 PLATFORM MODEL FOR THE EXPERIMENT [8]

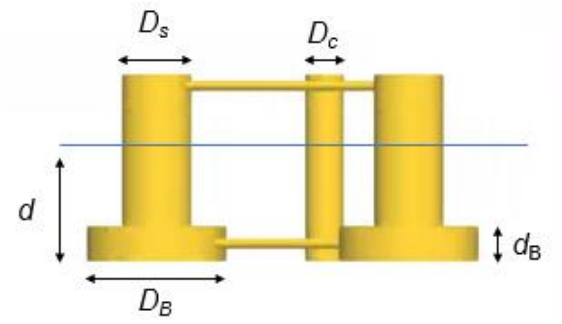

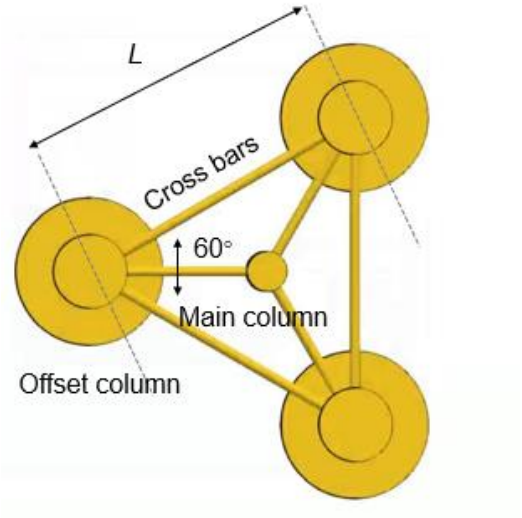

FIGURE 2: SKETCH OF THE SCALE MODEL GEOMETRY

TABLE 1: GEOMETRIC AND MOORING PARAMETERS

Geometric dimensions	
Main column diameter	Dc=0.09m
Offset Column diameter	Ds=0.165m
Base column diameter	DB=0.33m
Height of base column	dB=0.083m
Platform draft	d=0.27m
Distance between offset columns	L=0.688m
Inertia properties	
Mass of the Platform	m=36.7kg
Centre of mass	zc=-0.134m
Mooring parameters	
Stiffness in x direction	kx=27.5N/m
Stiffness in y direction	ky=28.1N/m

2.4 Numerical model

The dynamics of floating OC4 platform under current-only condition is firstly validated against the available experimental data summarised in Table 1. To reduce the complexity and computational time, the crossbars are omitted when we generate CFD mesh as shown in Figure 3. D is the characteristic dimension, which equals the diameter of the offset column D=D_s=0.165m. The platform locates at the centre of the x-y plane, with a distance of 14D between both side boundaries. The distance from the inlet and outlet boundary is 14D and 21D, respectively. Such distance is finalised via various numerical tests and proved to be sufficient to avoid the effect of sidewalls

on the computation results. The vertical distance between the centre of the platform and the bottom boundary is 7*D*.

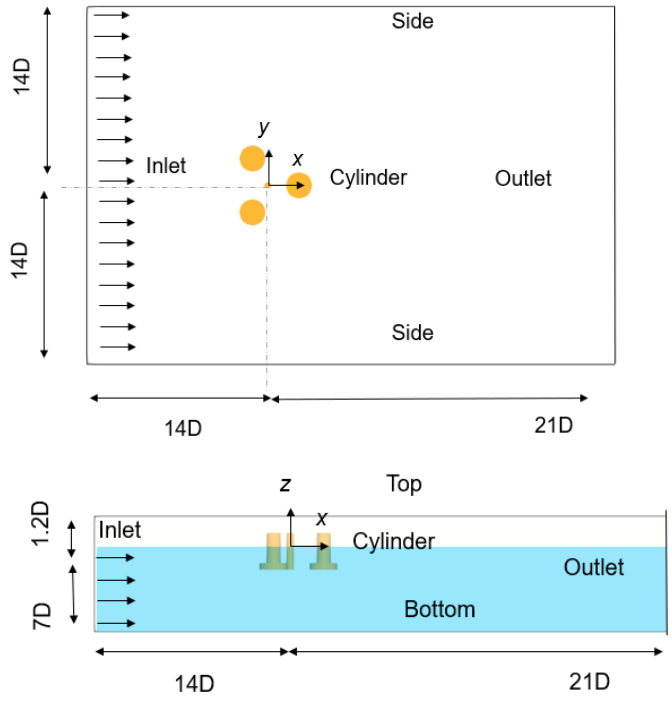

FIGURE 3: SKETCH OF THE NUMERICAL MODEL

The boundary conditions are set as follows: the zero-gradient condition for pressure is applied at the inlet boundary with the airspeed equals to zero, the pressure is set to zero at the outlet boundary. The fluid velocity at both inlet and outlet boundaries are given by a build-in boundary based on the wave theory, for the generation of wave-current and absorbing waves. An active absorbing outflow boundary is used to reduce the computational domain and cut time costs. Symmetry conditions are imposed at the side boundaries, and a no-slip condition is applied onto the platform walls so that the fluid velocity *U* at the platform surface is the same as the calculated platform velocity, and a non-slip boundary is applied at the bottom.

The unstructured mesh is used as displayed in Figure 4 and the mesh settings are as follows: 80 cells are uniformly distributed along the circumference of the platform, the height of the first cell layer on the platform surface is 0.01*D*, the total cell count is 3,500,000.

The time step is set to (1/800)*D*/*U* for all cases. PIMPLE (a combination of Pressure Implicit with Splitting of Operator (PISO) and Semi-Implicit Method for Pressure-Linked Equations (SIMPLE)) algorithm is utilized to solve the pressure-velocity coupling. A second-order Crank-Nicolson scheme is used for temporal discretization. Second-order upwind scheme is adopted for convective terms. Gradient terms are handled via a second-order cell-limited Gauss linear scheme.

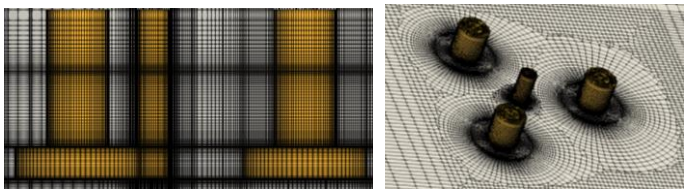

FIGURE 4: COMPUTATIONAL MESH FOR VIV SIMULATION

For the current only cases, the VIM of the platform is simulated with a variety of reduced velocities *V*r, which is defined as $V\mathrm{r} = U/f_\mathrm{n}D$, where f_n is the natural frequency. The parameters of the cases are listed in Table 2. For the wave-current test, only one wave parameter is examined.

TABLE 2: FLUID PARAMETERS FOR THE VIM TEST

Current Parameters							
U	0.08	0.11	0.13	0.14	0.16	0.2	0.24
*V*r	4.64	6.36	7.54	8.1	9.32	11.64	13.99
Wave Parameters							
Wave height				*H*=0.116m			
Wave Period				*T*=2.632s			

3. RESULTS AND DISCUSSION

The results are firstly compared with experiment data under current-only conditions as summarised in Figure 5. In Figure 5(a), where the motion response amplitude in cross-flow direction (A_y) is plotted, A_y is calculated by multiplying the root mean square (RMS) of the displacement by $\sqrt{2}$ and non dimensionalized by dividing characteristic length *D*. It is shown that the response amplitude agrees well with the experiment outside the lock-in regime from V_r=5 to 10. However, in the lock-in regime, although the reduced velocity, at which the peak A_y occurs, is very close, the A_y predicted by CFD is larger than the experiment. One possible reason for this discrepancy can be the absence of the cross-bars in the CFD numerical model. It is noted that the maximum response characterized by VIM is 0.57 times the column diameter, therefore, ignoring the cross-bars may decrease the motion drag from the surrounding fluid, and thus leading to a large motion. This is also consistent with the force analysis in Figure 5(b), where the lift coefficients from both CFD and experiment are compared.

Figure 6 shows the motion responses for wave-current-platform interaction at two given reduced velocities, i.e., V_r= 8.1 and 11.6, respectively. The simulation is performed by applying waves on top of current after *t*=140s current-only simulation. For V_r= 8.1, compared to the current-only cases, here, with the adding of waves, VIM is largely mitigated indicated by the appearances of the reduced motion amplitudes and irregular oscillations. For V_r= 11.6, more than one dominant frequency

can be observed in the displacement time history for current-only. When waves are applied, however, the VIM becomes regular with one predominant frequency which is higher than without wave.

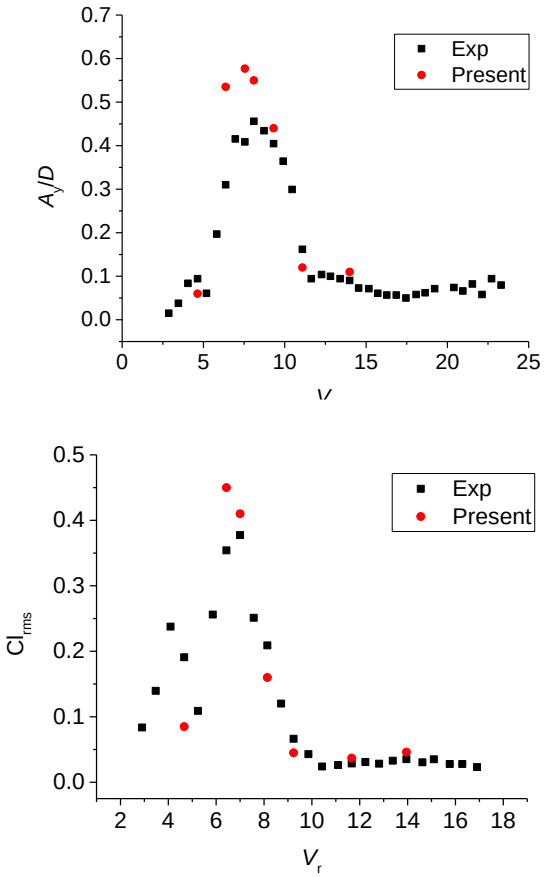

FIGURE 5: VARIATION OF (A) THE RESPONSE AMPLITUDE IN CROSS-FLOW DIRECTION AY/D, (B) RMS OF THE LIFT COEFFICIENT OF THE OC4 PLATFORM WITH THE REDUCED VELOCITY

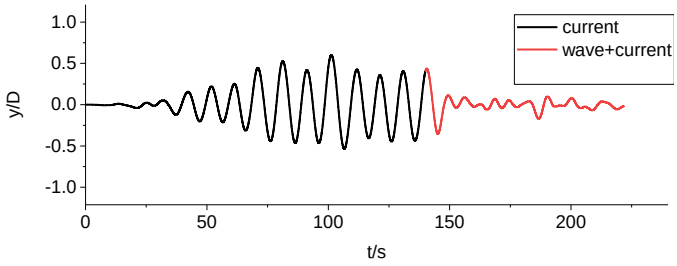

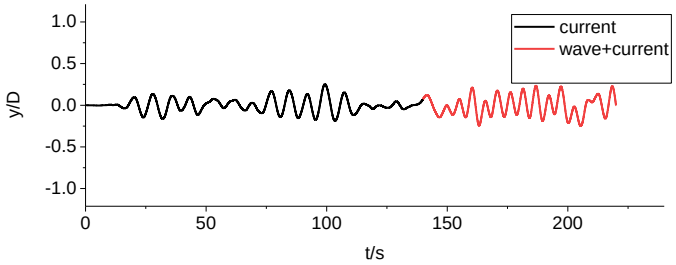

FIGURE 6: TIME HISTORIES OF THE RESPONSE FOR VIM OF THE OC4 PLATFORM FOR (A) V_r=8.1 INSIDE LOCK-IN REGIME (B) V_r=11.6 OUTSIDE LOCK-IN REGIME

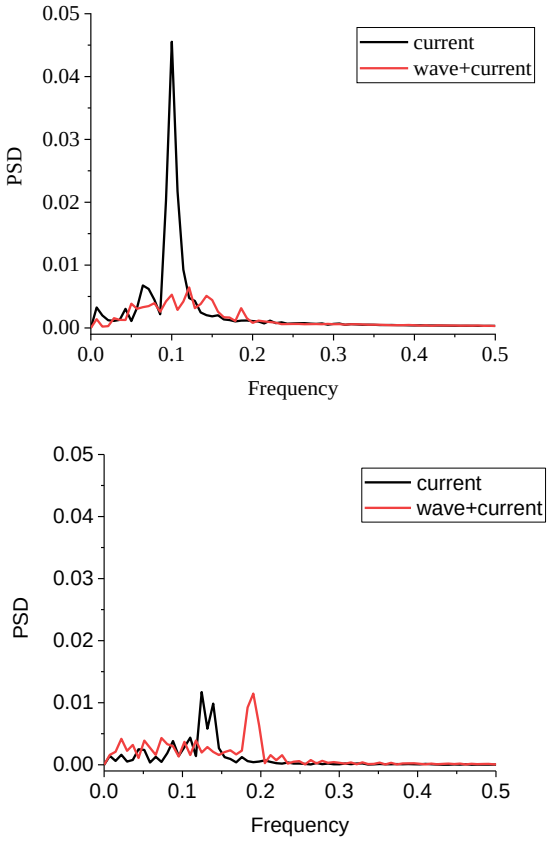

FIGURE 7: PSD OF THE RESPONSE FOR (A) V_r=8.1 (B) V_r=11.6 OF THE OC4 PLATFORM

The FFT analysis is performed to study the power spectra of the motion response. As shown in Figure 7, in the lock-in regime with V_r=8.1, the motion is excited at the natural frequency of 0.1Hz. With wave and current, the power distributes in a frequency domain ranging from 0.1Hz to 0.2Hz, and no evident dominant frequency is observed. Outside the lock-in regime with V_r=11.6, the energy is diminished, compared with that in the lock-in region. The dominant frequency increases with the increasing of V_r, which is consistent with the findings of Zhao et al [10]. With the interference of waves, the energy is no longer excited at a specific frequency near the natural frequency, it locates around 0.2*Hz* instead. This implies, given a large reduced

velocity, VIM does exist with wave incident even though the peak motion does not increase significantly in comparison with current only condition.

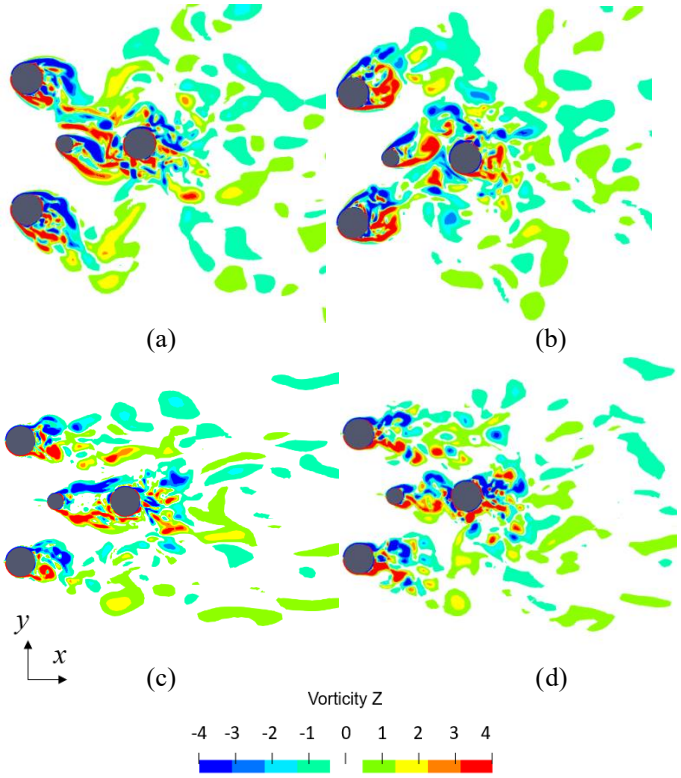

FIGURE 8: CONTOURS OF THE VORTICITY IN THE Z DIRECTION FOR V_r=8.1. (A) AND (B) CURRENT-ONLY CASES WHEN THE PLATFORM REACHES ITS MAXIMUM RESPONSE IN Y- AND Y+ DIRECTION; (C) AND (D) COMBINED WAVE-CURRENT CASES WHEN THE PLATFORM REACHES ITS MAXIMUM RESPONSE IN Y- AND Y+ DIRECTION

The vortex shedding structure can be visualised via the vorticity contour with our CFD results, as presented in Figure 8 and 9 for V_r=8.1 and V_r=11.6, respectively. Given the current only cases in Figure 8 (a) and (b), we can observe the vortices shed from two offset and the main columns with a classic 2S mode. They then encounter the third offset column, leading to a chaotic flow around columns. This makes the wake flow behind the column becoming very irregular. With adding of waves as shown in Figure 8 (c) and (d), the flow field is disturbed causing the vorticity becoming weaker, the vortex street changes from 2S mode to 2P mode. The vortex wake appears symmetric, and the vortex shedding occurs much earlier and closer to the columns. When V_r is creased to 11.6 shown in Figures 9 (a)-(d), the flow separation occurs much later than that of V_r=8.1, indicated by the vortex shedding points moving more downstream. Associated with that, a pair of symmetric shear layers separating from the two sides of the columns can be observed.

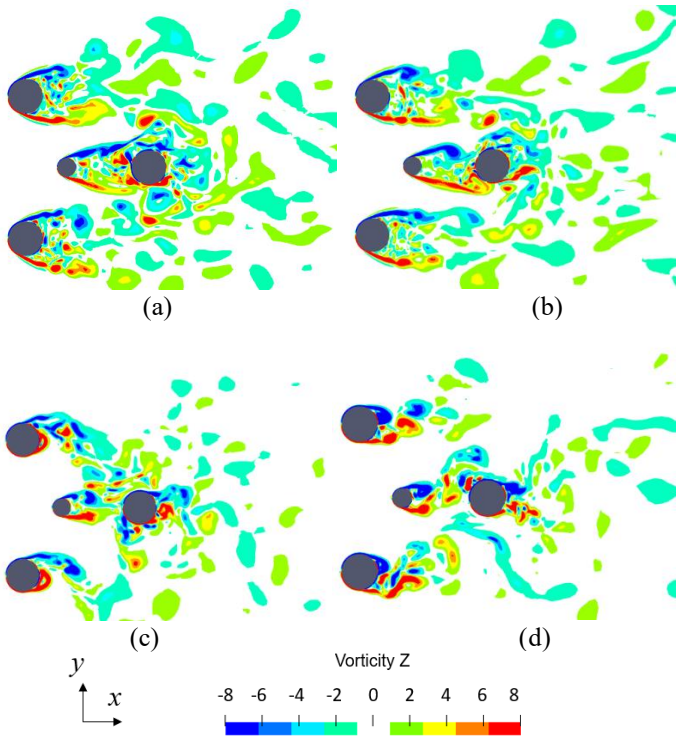

FIGURE 9: CONTOURS OF THE VORTICITY IN THE Z DIRECTION FOR V_r=11.6 (A) AND (B) CURRENT-ONLY CASES WHEN THE PLATFORM REACHES ITS MAXIMUM RESPONSE IN Y- AND Y+ DIRECTION; (C) AND (D) COMBINED WAVE-CURRENT CASES WHEN THE PLATFORM REACHES ITS MAXIMUM RESPONSE IN Y- AND Y+ DIRECTION

To better understand the three-dimensional vortex shedding characteristics, Figure 10 and Figure 11 display the evolution of the vortex structure with and without wave at V_r=8.1 using Q criterion of Q=0.8. Q is the second invariant of the rate of strain tensor. The contour color represents the velocity component along z-direction. Given a current-only condition, Figure 10 shows that Vortex 1 sheds from the upper-stream column, propagates downstream. The second vorticity, Vortex 2 generates from the edge of base column, propagates along its own x-y plane different from Vortex 1. The interaction between these two vortexes is rather small as indicated by the near-zero velocity component in z-direction. When the wave is added into current, as revealed by Figure 11, the flow particles are mixed up, the above-mentioned two vortices are broken down into more vortices with smaller size and strength. Because of the mixing along z-direction, the vortices herein also move up and down, leading to the strong dynamic motion of the platform in heave. The elevation of the wind-wave free-surface changes with time due to the adding of waves.

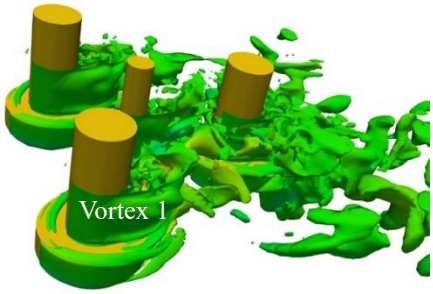

(a) t=134s

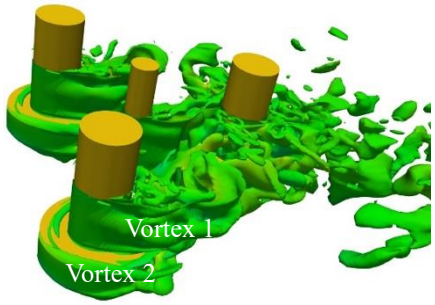

(b) t=136s

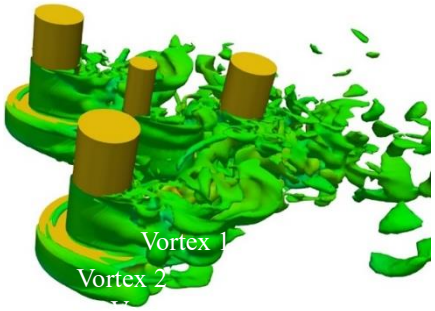

(c) t=137s

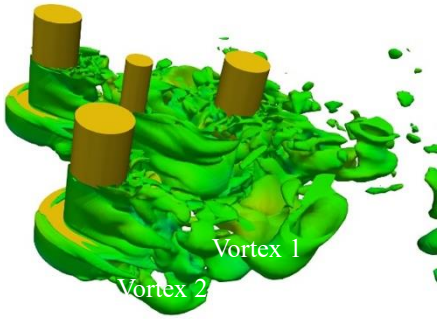

(d) t=139s

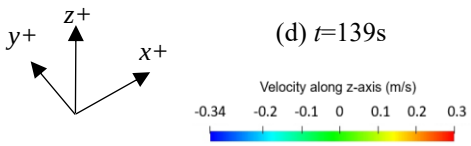

FIGURE 10: VORTEX EVOLUTION REPRESENTED BY ISO-SURFACE OF Q=0.8 AT V_r=8.1 WITH CURRENT ONLY, CONTOUR REPRESENT THE FLUID VELOCITY ALONG Z-AXIS

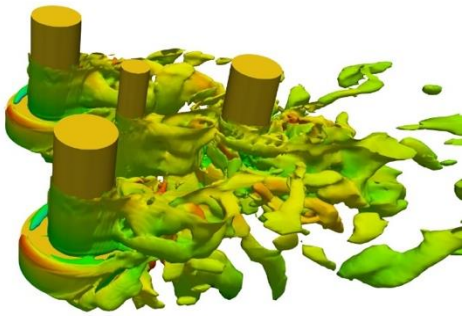

(a) t=212s

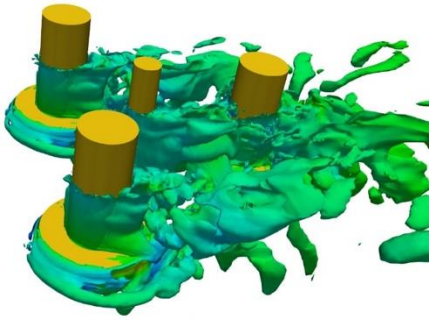

(b) t =213s

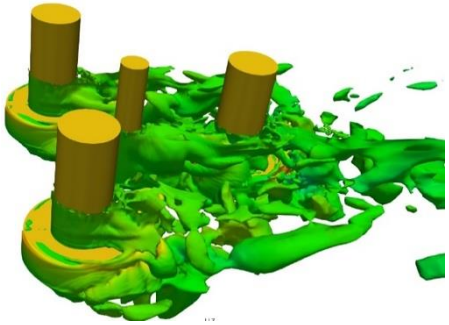

(c) t =214s

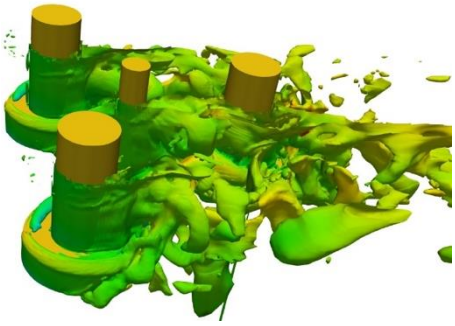

(d) t =215s

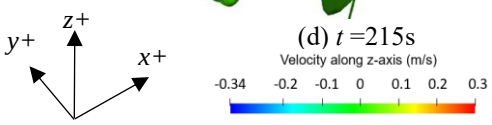

FIGURE 11: VORTEX EVOLUTION REPRESENTED BY ISO-SURFACE OF Q=0.8 AT V_r=8.1 WITH WAVES AND CURRENT, CONTOUR REPRESENT THE FLUID VELOCITY ALONG Z-AXIS

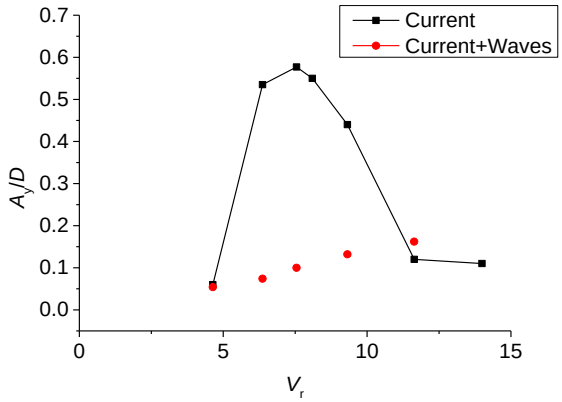

FIGURE 12: VARIATION OF THE RESPONSE AMPLITUDE IN CROSS-FLOW DIRECTION AY/D WITH WAVES AND CURRENT

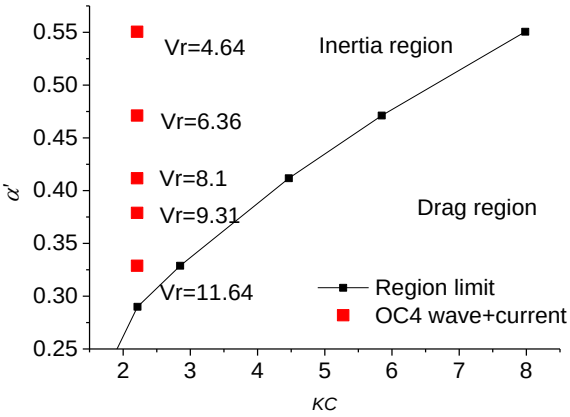

FIGURE 13: *α-KC* PLOT DENOTING PREDOMINANT REGION OF EITHER DRAG OR INERTIA FORCE WITH CURRENT AND WAVES FOR OC4 PLATFORM

A comparison of VIM response with and without waves is made in Figure 12. It can be seen that, with the wave parameters studied, the VIM response decreases as compared to current-only cases in the lock-in regime. Outside this regime, there are no obvious differences between with or without waves. It has to be pointed out that only one wave condition is studied in this paper, therefore, it's not clear whether the above conclusion could be applied to other wave-current conditions. Previous work by Iwagaki and Asano [15] for VIV of cylinder and by Gonçalves et al. [13, 14] for VIM of multi-column floater revealed that the VIM induced by wave is governed by both viscous or inertia forces. The ratio between these two forces is given the name of velocity ratio α', which can quantify whether a flow is viscous or inertial dominant. This can be further illustrated by a plot of velocity ratio α' as a function of the Keulegan-Carpenter number, KC, as shown in Equations (9) - (10).

$$\alpha' = \frac{\sigma_U}{\sigma_U + U_c} \tag{9}$$

$$KC = \frac{U_M}{f_w D} \tag{10}$$

where U_M is the maximum flow velocity of the in-line motion of the platform, U_c is the current velocity, σ_U is the RMS value of the in-line motion of the platform.

Their relationship can be seen in the *α-KC* plot in Figure 13. The black line denotes the threshold between drag range and inertia range. It can be seen that, for the wave parameters studied in this paper, most cases are in the inertia regime, thus the VIM response is more or less mitigated with the adding of waves. To extend this conclusion to a wide range of wave-current and platform parameters, further study is needed.

4. CONCLUSION

The wave-current-structure interaction for OC4 semi-submersible platform is studied using CFD method. The VIM response in the cross-flow direction of the platform has a good agreement with the experiment. In the lock-in regime, the maximum cross-flow motion is 0.6 times the column diameter, which represents a strong VIM effect. With the given incident waves, the VIM is mitigated for most cases, for a wide range of reduced velocity. This mitigation becomes weaker for VIM with higher reduced velocity, for which the *α-KC* plot denotes the VIM is closer to the drag-inertia force threshold. An examination of the vorticity field shows that wave changed the pattern of the vortex shedding, making the separation process of vertex more unstable. These results suggest the VIM could be neglected in industrial design applications, even if studies on a larger range of wave conditions and on different floater geometries would be necessary to fully confirm this point.

REFERENCES

[1] Bao, Y., Huang, C., Zhou, D., Tu, J., and Han, Z., 2012, "Two-degree-of-freedom flow-induced vibrations on isolated and tandem cylinders with varying natural frequency ratios," Journal of Fluids and Structures, 35, pp. 50-75.

[2] Gonçalves, R. T., Rosetti, G. F., Franzini, G. R., Meneghini, J. R., and Fujarra, A. L. C., 2013, "Two-degree-of-freedom vortex-induced vibration of circular cylinders with very low aspect ratio and small mass ratio," Journal of Fluids and Structures, 39, pp. 237-257.

[3] Zhao, M., and Cheng, L., 2014, "Vortex-induced vibration of a circular cylinder of finite length," Physics of Fluids, 26(1).

[4] Cueva, M., Fujarra, A. L., Nishimoto, K., Quadrante, L. s., and Costa, A. P., "Vortex-induced motion: model testing of a monocolumn floater," Proc. International Conference on Offshore Mechanics and Arctic Engineering, pp. 635-642.

[5] Gonçalves, R. T., Fujarra, A. L., Rosetti, G. F., and Nishimoto, K., 2010, "Mitigation of vortex-induced motion (VIM) on a monocolumn platform: forces and movements," Journal of offshore mechanics and arctic engineering, 132(4).

[6] Sagrilo, L. s. V. S., Queija de Siqueira, M., Gonc¸alves de Lacerda, T. A. n., Ellwanger, G. B., Castro Prates de Lima, E., and Siqueira, E. F. N., "VIM and wave-frequency fatigue damage analysis for SCRs connected to monocolumn platforms," Proc. International Conference on Offshore Mechanics and Arctic Engineering, pp. 723-729.
[7] Gonçalves, R. T., Rosetti, G. F., Fujarra, A. L. C., and Oliveira, A. C., 2012, "Experimental study on vortex-induced motions of a semi-submersible platform with four square columns, Part I: Effects of current incidence angle and hull appendages," Ocean Engineering, 54, pp. 150-169.
[8] Gonçalves, R. T., Chame, M. E. F., Silva, L. S. P., Koop, A., Hirabayashi, S., and Suzuki, H., 2021, "Experimental Flow-Induced Motions of a FOWT Semi-Submersible Type (OC4 Phase II Floater)," Journal of Offshore Mechanics and Arctic Engineering, 143(1).
[9] Kim, J.-W., Magee, A., and Guan, K. Y. H., "CFD simulation of flow-induced motions of a multi-column floating platform," Proc. International Conference on Offshore Mechanics and Arctic Engineering, pp. 319-326.
[10] Zhao, W., Zou, L., Wan, D., and Hu, Z., 2018, "Numerical investigation of vortex-induced motions of a paired-column semi-submersible in currents," Ocean Engineering, 164, pp. 272-283.
[11] Huang, H., and Chen, H.-C., 2020, "Investigation of mooring damping effects on vortex-induced motion of a deep draft semi-submersible by coupled CFD-FEM analysis," Ocean Engineering, 210.
[12] Maximiano, A., Koop, A., de Wilde, J., and Gonçalves, R. T., "Experimental study on the vortex-induced motions (VIM) of a semi-submersible floater in waves," Proc. International Conference on Offshore Mechanics and Arctic Engineering, American Society of Mechanical Engineers, p. V07BT06A016.
[13] Gonçalves, R. T., Pinto, L. A., and Fujarra, A. L. C., 2020, "Experimental study on vortex-induced motions of a semi-submersible platform with four square columns, part III: Effects of the collinear irregular and regular wave incidence and current," Ocean Engineering, 217.
[14] Gonçalves, R. T., Rosetti, G. F., Fujarra, A. L. C., and Oliveira, A. C., 2013, "Experimental study on vortex-induced motions of a semi-submersible platform with four square columns, Part II: Effects of surface waves, external damping and draft condition," Ocean Engineering, 62, pp. 10-24.
[15] Yuichi, I., and Toshiyuki, A., 1984, "HYDRODYNAMIC FORCES ON A CIRCULAR CYLINDER DUE TO COMBINED WAVE AND CURRENT LOADING," Coastal Engineering Proceedings, 1(19).